Pore-scale oxygen (O_2) dynamics of vadose zone under dry-wet cycles of artificial recharge: A soil lysimeter experiment

Tanushree Dutta[a,*], Albert Carles-Brangarí[a], Daniel Fernàndez-Garcia[a], SimonettaRubol[a,b], Joel Tirado-Conde[a], Xavier Sanchez-Vila[a]

[a]*Hydrogeology Group, Department of Geotechnical Engineering and Geosciences, Universitat Politècnica de Catalunya - BarcelonaTech, Spain*

[b]*Department of Mechanic, Civil and Environmental Engineering, University of Trento, Italy*

[*]Corresponding author: *tanushree.dutta@upc.edu (T.Dutta)*

ABSTRACT

Vadose zone oxygen dynamics control all subsurface redox reactions and play a decisive role in maintaining groundwater quality. Although drying and wetting events are common in artificial recharge, their effects on subsurface oxygen distribution are poorly documented. We monitored oxygen concentration in the unsaturated zone in a mid-scale (1 m high) laboratory soil lysimeter, which was subjected to short wetting and drying cycles that simulated a highly permeable shallow aquifer recharged by river water. Ten cycles of varying duration were performed for a period of 85 days. Measurements of oxygen in the liquid and the gas phases were recorded every 20 seconds using non-invasive optical fibers (PreSens). The results provided high-resolution (in time) oxygen concentration maps. The infiltration rate revealed a decreasing trend during wetting cycles associated with biological clogging. Such a decrease with time was accompanied by a depletion of O_2 concentration, occurring within the first few hours of the

infiltration. During drying, O_2 concentrations recovered rapidly at all depths owing to air flushing, resulting in a stratified vertical profile consistent with the biological consumption of O_2 along the air infiltration path. Furthermore, drying periods caused a potential recovery of the infiltration capacity while preserving the soil biological activity. Scraping also led to the recovery of the infiltration capacity of the soil but was less effective than drying. Our experiment suggests that the small-scale heterogeneity played a key role in accurately mapping pore-scale O_2 concentrations and should be considered in modeling O_2 fluxes of unsaturated soils under natural or managed recharge conditions.

Keywords: Oxygen concentration dynamics, precision sensing, Managed Aquifer Recharge, infiltration, drying-wetting cycles, biological processes

HIGHLIGHTS

- Successive wet-dry cycles of artificial recharge alter the infiltration rates with time
- Oxygen concentration stabilizes within few hours of commencement of infiltration and drying
- Drying restores the infiltration rate close to its initial value
- Surface scraping results in an immediate but temporary increase in the infiltration rate
- Quantifying small changes in space and time is vital for accurate pore-scale O_2 mapping

41 **1. Introduction**

42 Subsurface redox zonation is driven by the spatial and temporal distribution of oxygen that
43 serves as the primary terminal electron acceptor during the degradation of organic carbon
44 (Greskowiak et al., 2006). Understanding oxygen zonation in artificial recharge is important for
45 two reasons: (a) biodegradation of hydrocarbons demands aerobic conditions (Rifai et al., 1995;
46 Christensen et al., 2000), and (b) biodegradation of halogenated compounds requires reducing
47 conditions (Bouwer, 1994; McCarthy and Semprini, 1994; Vogel, 1994). Moreover, bio-
48 denitrification takes place preferentially under anaerobic conditions (Schmidt et al., 2011; Rubol
49 et al., 2012). Thus, in order to better understand organic and inorganic contaminants in aquifer
50 systems, it is necessary to carry out a detailed mapping of the subsurface distribution of oxygen
51 and to elucidate the transport processes. Artificial recharge of groundwater from available
52 surface water is an important management strategy for replenishing groundwater supplies while
53 improving water quality (Dillon, 2005; Fox et al., 2006). The extent to which conditions in these
54 managed systems can be optimized to achieve an adequate water supply (involving both
55 quantity and quality aspects) depends largely upon the physical, geochemical and biological
56 processes that occur in the vadose zone.

57 Application of surface water or wastewater in rapid infiltration systems is cyclic and typically
58 consists of a period of water application (flooding) followed by days or weeks of drying (Bouwer
59 and Rice, 1984; NRMRI, 2006; US EPA, 1984). Drying is often accompanied by scraping the low-
60 permeability layer on the pond's floor (e.g., Mousavi and Rezai, 1999). This is a way to recover
61 aerobic conditions of the topsoil surface and the infiltration capacity, and to renew the soil´s
62 capability of biodegradation (e.g., Bouwer, 2002). The hydraulic loading rate within each wetting
63 cycle affects oxygen availability, pore-fluid velocity and retention time. However, it is not

64 possible to assess the optimal ratios of flooding/drying periods owing to the complexity and
65 difficulty in accurately measuring and mapping the spatial and temporal distribution of oxygen
66 concentrations in the field (Akhavan et al.,2013).

67 Soil pore oxygen concentration depends on the interaction between transport and consumption
68 processes. The former is regulated by advection and diffusion, whereas the latter occurs via
69 chemical reactions and microbial activity. Hot-moments, which are defined by McClain et al.
70 (2003) as short periods that display very high reaction rates with respect to longer intervening
71 periods, affect microbial activity directly (Schimel et al., 2007) or indirectly by changing the
72 redox conditions and O_2 availability (e.g., Rubol et al., 2012). High resolution O_2 maps of soil
73 metabolic activity revealed the presence of these hot-moments in riverbed sediments (Dutta
74 and Rubol, 2014). Microbes can adapt to fluctuations of redox conditions by changing their
75 function or composition (DeAngelis et al., 2010), or protecting themselves by forming biofilms
76 (Romaní et al., 2004). Biofilm formation may result in biological clogging, which could reduce the
77 hydraulic conductivity of the soil by several orders of magnitude (Baveye et al., 1998; Bouwer
78 and Rice, 2001) and alter the soil's water retention capacity (Rubol et al., 2014). Infiltration rates
79 may also be affected by temperature, either directly due to the dependence of water viscosity
80 on temperature (Constantz, 1982; Jaynes, 1990), or indirectly as temperature affects biological
81 activity (Le Bihan and Lessard, 2000). Notwithstanding, a poor knowledge of the pore-scale
82 processes and the lack of instrumentation techniques to capture small-scale heterogeneity
83 prevents us from proper upscaling from micro to larger macro scale (Krause et al., 2014).

84 In the present study, using a 1m high lysimeter equipped with an array of sensors, we monitored
85 a number of physical and chemical parameters continuously over a period of 85 days in order to
86 link the spatial and temporal dynamics of fluid flow, water retention, and pore-scale O_2

87 concentration distribution with depth and time during the succession of wetting and drying
88 cycles. The experimental setup also allowed us to assess the changes in the infiltration capacity
89 resulting from the drying phases.

90

91 **2. Materials and Methods**

92 *2.1. Soil Collection, Preparation and Characterization*

93 Soil was collected from the prodelta region of the Llobregat River in a Managed Aquifer
94 Recharge facility located in Sant Vicenç dels Horts, Spain (418446.63 N, 4581658.18 E, zone 31T).
95 Pebbles and coarse grains were removed by passing the soil through a sieve of 0.2 cm. As a
96 result, the amount of fine grains increased, facilitating permeability and the soil's capacity to
97 generate bacterial activity. By using a sieve of 0.2 cm, the architecture of soil aggregates was
98 preserved.

99 Representative soil samples were analyzed for particle size distribution, pH and dissolved
100 organic carbon (DOC, organic carbon analyzer model Shimadzu TOC-V-CSH 230V). A small
101 composite sample was extracted using 2M KCl for the determination of ammonium and nitrate.
102 The extractants were analyzed using an Ionic chromatograph (model-DIONEX IC5000) equipped
103 with an autosampler with an eluant flow rate 1 mL/min, an IonPac® AS18 anion-exchange
104 column (4x250mm) with an AG Guard column (4x50 mm) and an IonPac® CS16 cation-exchange
105 column (5x250mm) with a CG Guard column (5x50 mm).

106 Analysis of particle size distribution (ASTM, 2000) indicated that the soils were largely composed
107 of medium sand (>80%, see Table 3). X-ray powder diffraction analysis of a sample of soil
108 located nearby revealed that the soil consisted mostly of quartz, with an observable amount of

109 calcite and traces of dolomite, albite, clinochore, muscovite and orthoclase (exact proportions
110 not known). Chemical characteristics of the sediment are listed in Table 3.

111 *2.2. Lysimeter Set-up, Packing and Chemical sink addition*

112 A rectangular shaped lysimeter was constructed following the method described in Rubol et al.
113 (2014) (see Fig 1 for the complete setup). The lysimeter was made of plexiglass, and was 1.2 m
114 high, 0.46 m long, and 0.15 m wide to minimize boundary effects and to allow for some degree
115 of heterogeneity in both the vertical and horizontal directions. All the instrumentation and
116 materials (except the soil) were autoclaved.

117 The lower 15 cm of the tank was filled with silica sand (0.7 to 1.8 mm diameter, supplied by
118 Triturados Barcelona, Inc.) and was covered with a geo-synthetic membrane to prevent flushing
119 of the smaller particles out of the system. The upper 85 cm of the tank was filled with the sieved
120 soil to minimize perturbations both in soil conditions and existing cellular biodiversity. Granular
121 materials were placed layer by layer (10 cm thick) and were packed manually to attain an
122 adequate consistency. Additional compaction occurred owing to the hydrostatic forces created
123 by successive filling and emptying of the device but no additional shrinkage was observed. Filling
124 took place from the bottom to avoid bubble retention. Porosity values were determined from
125 the saturated water content, ranging from 0.27 to 0.38 depending on the sensor location. An
126 initial dry bulk density of 1.38 g/cm^3 was measured.

127 The top 20 cm of the tank was left empty to allow ponding and infiltration conditions to develop
128 during wetting periods. The height of the water above the soil surface was maintained at a fairly
129 constant level by means of a regulated peristaltic pumping system. Using this device, the system
130 was fed with chemically controlled (synthetic) water with no recirculation. The synthetic water
131 was made up of the chemical signature compounds of the river Llobregat (see Table 1). Organic

and inorganic compounds (see Table 1 for compositions) were mixed with deionized water daily in order to minimize variations in its chemical composition with time. To monitor the infiltration rate, pumped water and water level at the pond were recorded. Infiltration as a function of time was estimated by applying water balance considerations at the pond. The rate of evaporation during the wetting phases was negligible compared with the infiltration rate. During drying periods, the water feeding system was substituted by an array of five 15W light bulbs. These bulbs were placed 15cm above the surface to mimic the effect of the sun directly on the soil surface during the drying phases. Only the surface of the lysimeter was directly exposed to light, while the lateral walls were covered by a black plastic bag to prevent autotrophic activity inside the system. The bottom of the tank was connected to an external water reservoir to fix the water table level.

2.3. Experimental protocol and Data collection

The infiltration experiment lasted 85 days. By changing the top boundary condition, the lysimeter was subjected to five wetting (W) cycles alternating with five drying (D) cycles of variable duration (see Table 2). The cycles can be classified according to their duration as: medium (W1-D1, W2-D2), long (W3-D3, W5), and short (W4-D4, D5). In the middle of the longest wetting cycle, W3, infiltration was discontinued for a short time, followed by scraping of the top (about 5 cm) before wetting was resumed. This is shown as two distinct cycles in Table 2: W3a, W3b.

Three types of sensors were placed: 5 capacitance sensors (5TE, Decagon Devices) to measure volumetric water content and temperature at depths 5, 15, 30, 45 and 58 (all depths are reported in cm measured from the topsoil); 5 tensiometers (three T5, UMS; and two MPS-2, Decagon Devices) to measure soil water potential also at depths 5, 15, 30, 45 and 58; 2 pressure

155 transducers (Mini-Diver, Schlumberger) to monitor the water table placed at the top and
156 bottom; a third pressure transducer (Baro-Diver, Schlumberger) to record atmospheric
157 variations; and several non-invasive optical sensors (PreSens) to measure partial pressures of
158 oxygen and carbon dioxide (both dissolved and in gas phase). O_2 sensors were placed at depths
159 5, 15 (2 sensors), 30 (2), 45, 58 (2), plus inlet and outlet, while CO_2 sensors were located at
160 depths 15, 45, inlet and outlet. Measurements of gas phase sensors were corrected to
161 compensate for temperature effects. Figure 1 shows the location of the different sensors.

162

163 **3. Results: Temporal evolution of infiltration Rates**

164 In each wetting cycle, a quasi-exponential reduction in the infiltration rate with time was
165 observed except for a brief period at the beginning of the experiment, when the system had to
166 adapt to the sudden change in the hydraulic conditions. The time evolution of infiltration rates is
167 presented in Figure 2. During W1 the infiltration rate slightly increased from 200 to 240 L/day. In
168 the remaining wetting cycles, a general trend was observed starting from an initial high value
169 just after the beginning of the cycle, which then decreased rapidly. For example, by the end of
170 W2 the infiltration rate was down to 100 L/day, and was as low as 12 L/day by the end of W5.
171 W4 was too short to observe a decrease in the infiltration rate. At the beginning of all wetting
172 phases the infiltration rate was larger than 200 L/day, indicating a brief period of recovery of the
173 system at the end of each drying period. After scraping in W3, the infiltration rate suddenly
174 recovered, rising from 40 to 200 L/day before decreasing again.

175 During wetting conditions the water content in the soil approached the porosity values,
176 indicating a high saturation condition. During drying, the water content fell to values, ranging
177 between 0.1 and 0.2, which resulted in capillary pressures that did not exceed 0.2 MPa.

178

179 **4. Results: Oxygen dynamics**

180 O_2 concentrations displayed distinctive trends both in depth and time associated with the
181 different drying and wetting cycles (Figure 3). Concentrations measured at the pond were
182 always below saturated conditions in equilibrium with the atmosphere, yet higher than those
183 recorded at any sensor within the lysimeter. Oxygen depletion at ponds associated with
184 biological activity has been reported elsewhere (Greskowiak et al., 2005).

185 *4.1. Wetting cycles*

186 During W1, O_2 concentration in the ponding area remained consistent between 8 to 9 mg/L
187 (Figures 3, 4). In the soil, however, during the first 24 h of infiltration, redox conditions
188 underwent a drastic shift. After a transient period when oxygen concentration decreased at all
189 depths, a well-stratified profile of decreasing oxygen with depth was established (Figure 4).
190 Subsequently, O_2 concentration at each depth remained consistent with time.

191 A similar trend of O_2 concentration was observed at the beginning of W2 with respect to W1,
192 the only difference being the faster depletion of O_2 at depths below 5 cm. O_2 concentrations
193 were consistently low except on day 14 (one day after the start of W2) when a spike of O_2 was
194 observed at all depths, albeit more pronounced near the surface. After day 14, O_2 levels
195 decreased at all depths making the system almost completely anoxic by day 15. Oxygen
196 concentrations in the pond and soil during W3 were consistent with those in W2 except for a
197 faster depletion in the former. Even though a small spike of O_2 was observed a day after the
198 start of W3, the soil remained mainly anoxic for the first four days. A longer spike appeared on
199 day 31 (Figure 3). During scraping (day 34), oxygen levels recovered at all depths. Thereafter, O_2

200 concentration decreased in an approximately exponential rate but at a slower rate than those
201 observed in the previous wetting phases. Despite W4 follows a long drying period, D3, this
202 wetting cycle showed a dynamic behavior similar to W1 in terms of O_2 distribution. Finally, in
203 W5 O_2 concentration decreased rapidly at all cross-sectional depths, showing a behavior similar
204 to W2 and W3. An unexpected oxygen pulse entered the system on day 78.

205 *4.2. Drying cycles*

206 Figure 5 shows the time evolution of the oxygen in the pond at different depths for the first 5
207 days after the start of the drying cycles. The partial pressure of O_2 in the ponded water was
208 fairly consistent at 200 hPa for all cycles. The distribution of O_2 along the vertical cross-section
209 lysimeter did not vary much between the 5 drying cycles, displaying very similar distribution
210 patterns. During the first hours of each drying period, oxygen concentrations at all depths
211 recovered rapidly approaching a vertical profile with a clear stratification. Re-oxygenation was
212 slower at greater depths, but eventually oxygen partial pressure reached atmospheric levels at
213 all depths. However, at steady state conditions, partial pressure of soil O_2 remained just below
214 200 hPa.

215

216 **5. Interpretation of results and discussion**

217 *5.1. Effects of wetting, drying and removal of surface layer on water infiltration dynamics*

218 The infiltration capacity of the system, although roughly constant, increased slightly during W1.
219 This effect may be related to the physical rearrangement of the grain particles at the micro-scale
220 at the start of wetting. Since the soil was hand-packed, the initial water flow rearranged particle

221 locations, generating a new pore distribution and some small scale preferential pathways that
222 changed the overall hydraulic conductivity during the first few days.

223 After W1, the time evolution of measured infiltration rates during wetting cycles displayed an
224 approximate exponential decrease, down to 60% after W2 and 85% after W3 with respect to the
225 original values at the start of each corresponding cycle. Similar exponential-like decreases in
226 infiltration rates have been reported elsewhere, and are attributed to the decline in
227 permeability because of clogging (e.g., Bouwer, 1978; Pedretti et al., 2012). One result of
228 clogging is a significant decrease in pressure heads in the vertical cross-section below the soil
229 surface where the maximum microbial colonies form (Bouwer, 2002). Of significance is the rate
230 of oxygen depletion during wetting (in absolute value) in W1 with respect to other cycles.

231 These observations could be attributed to the presence of EPS (extracellular polymeric
232 substances), which are capable of reducing hydraulic conductivity, thus causing clogging
233 (Vandevivere and Baveye, 1992; Thullner et al.,2002). Although not measured in this test, the
234 presence of EPS was observed in the infiltration experiment performed by Rubol et al. (2014)
235 with soil from the same site. Rubol et al. (2014) reported that the soil infiltration capacity
236 decreased during continuous infiltration with significant increase in the water holding capacity
237 at greater depths, where the presence of EPS was more marked. During W1, microbial colonies
238 probably develop (this being quite a relatively slow process). After W2, colonies did not
239 necessarily grow anymore, but EPS were excreted with time, leading to clogging. During the
240 drying phases, the infiltration capacity in the lysimeter reverted to its original value, as EPS
241 reduced its volume. However, the living microbial cells remained active protected from
242 desiccation by EPS (Or et al., 2007).

When the system was re-wetted, a fast recovery of the biological activity was observed in the oxygen profile (Figure 4). A plausible explanation for this occurrence is that the bacterial colonies, still active despite the low water content, had to reactivate or readapt themselves to the increase in water availability under very favorable conditions (presence of water and nutrients).

The infiltration capacity of the system increased following the scraping of the top surface layer (in W3), but it did not reach the value recorded at the start of W3, probably because scraping only affected the top surface whereas clogging occurred at all depths. The subsequent decrease in the infiltration rate with time was again exponential but at a slower rate than at the start of W3. This means that scraping had effectively disturbed the first centimeters of the soil and that the impact of clogging upon permeability continued to be felt. These results are in agreement with those of Mousavi and Rezai (1999), who evaluated the effect of scraping in three artificial recharge basins and found that the treatment was only partially efficient, i.e. restoration of only 68% of the initial infiltration rate. Note, however, that at the start of W4, the infiltration capacity increased again to a high value, suggesting that desiccation is more effective than scraping in terms of infiltration rate recovery.

5.2. O_2 concentration dynamics and changes in biological activity during wetting and drying

Dynamics of O_2 concentrations within the lysimeter during wetting and drying cycles can be attributed to three main processes: flow advection, diffusion in the air phase and O_2 consumption. Once the infiltration front reaches the sensor by advection after the start of a wetting cycle, oxygen concentrations rapidly decline with time owing to biological activity. This is corroborated by the soil CO_2 respiration activity (Figure 7). Figure 6 shows that depletion of

oxygen is modeled as a negative exponential function with a first-order decay parameter (λ), which indicates the velocity of the system needed to achieve anoxic conditions:

$$C_{O_2} / C_{O_2,0} = \exp(-\lambda \frac{t}{t_{adv}}) \quad (1)$$

where, $C_{O_2,0}$ is the oxygen value at the surface boundary (z=0), t is time and t_{adv} is the characteristic time of advection based on the flow velocity. The estimated values of λ ranged between 0.0044 (wetting cycle W3b) and 0.0427 (wetting cycle W3a). Hence, at the start of the third wetting cycle, the rate of oxygen consumption was the highest but the value dropped to a minimum after the scraping.

Drainage marks the start of each drying cycle with the result that the advective flow of gas rapidly occupies the pore spaces previously filled by water. After about 3 h of drying, the system reached quasi steady state oxygen conditions displaying a well-defined vertical gradient. A distribution that is characteristic of a combination of diffusion and decay (biological consumption). Assuming that oxygen in air and residual water are in equilibrium, the partial pressure of oxygen, P_{O_2} is governed by

$$D \frac{\partial^2 P_{O_2}}{\partial z^2} - k P_{O_2} = 0 \quad (2)$$

where, D is the effective diffusion coefficient of O_2 [L^2T^{-1}] and k is the first-order de-oxygenation rate based on consumption due to bacterial activity. Integration of this equation gives an exponentially decaying oxygen profile from the value at the surface $P_{O_2,0}$

$$P_{O_2} = P_{O_2,0} \exp(-\sqrt{k / D}\, z) \quad (3)$$

From (3), a characteristic depth (d) can be defined as

$$d = \sqrt{D/k} \quad (4)$$

An effective diffusion coefficient of oxygen of D = 0.0068 cm^2/s was estimated from the Millington and Quirk (1961) model with a gas content of 0.2 and a diffusion coefficient of oxygen in air of 0.2 cm^2/s. Using a characteristic depth d between 20 and 40 cm (other values could be employed here with slightly different results) in equation (4), the first-order de-oxygenation constant k ranges between 1.5 and 0.36 day^{-1}.These values are surprisingly similar to the first-order decay coefficients λ obtained by analyzing the de-oxygenation rates observed in Figure 4 during wetting cycles. This result indicates that the soil was biologically active both during drying and wetting periods. Roberson and Firestone (1992) and Zhang and Yan (2012) reported that bacterial activity remained consistent during both wetting and drying cycles, suggesting that desiccation does not exert a significant effect on cell activity. It should be pointed out that the overall cell activity probably decreased due to the drop in the availability (amount and diversity) of electron acceptors but the activity remained almost intact owing to the availability of oxygen. Given that EPS formation was observed in another infiltration experiment performed with the same soil type (Rubol et al., 2014), we believe that the microbial activity was probably protected by the presence of EPS during drying cycles.

The dynamics between O_2 consumption, biological activity and advection are responsible for a slower reduction of oxygen concentrations during wetting periods compared with the rise in drying periods. The factors influencing the rate of re-aeration are soil type, soil oxygen demand and vadose zone thickness (Neale et al., 2000; Rubol et al., 2013). The high sand percentage in the lysimeter (>99%) was probably instrumental in the high oxygen concentration values reported (Fetter, 1990).

307 *5.3. Relevance of the frequency of monitoring O_2 dynamics*

308 In order to illustrate the effect of oxygen sampling on bio-growth estimates, we employed
309 Monod kinetics to model the rate of growth of biomass using substrate O_2 as the limiting factor.
310 The governing equation is written as

311 $$\frac{dX}{dt} = \mu_{\max}\left(\frac{C_{O_2}}{K_{O_2} + C_{O_2}}\right)X - K_d X \qquad (5)$$

312 Where X is the cell biomass concentration, $\mu_{\max}$ is the kinetic coefficient for the maximum
313 specific growth rate, C_{O_2} is the dissolved oxygen concentration, K_{O_2} is Monod's half-saturation
314 constant for dissolved oxygen, and K_d is the parameter to account for the endogenous decay
315 of the biomass. All parameters used in the following simulations (reported by Shaler and Klecka,
316 1986) are displayed in Figure 8.

317 The accuracy of the model used for prediction of the rate of biodegradation reactions is
318 considerably improved by the high frequency of measurements. Figure 8 (top) illustrates the
319 variability in dissolved oxygen as a function of time. This is depicted in three sampling strategies
320 in a period close to 3.5 days and corresponding to W1. The figure displays the complete data set
321 recorded by one sensor at a very high frequency (one value every 20 seconds) located at the
322 depth of 5 cm, and two more sensors recording at a relatively low frequency (one value every
323 4.2 h or 1.16 days, respectively). The main trend of decreasing oxygen concentration with time is
324 observed in all the curves but strong local fluctuations are not shown in the coarser sampling
325 protocols.

326 Figure 8 (middle) shows the importance of the sampling strategy in terms of the sensitivity of
327 biomass concentration derived from (5) as a function of sampling strategy. Because of the

328 chosen values of the modeling parameters during rewetting cell biomass undergoes little change
329 regardless of our ability to properly characterize oxygen concentrations. The main reason for
330 this is that $C_{O_2} > K_{O_2}$, the latter being equal to 1.2 mg/L. As a consequence, the solution of (5)
331 is very close to an exponential curve, where the increase is caused by $\mu > K_d$.

332 By day 2.5 there is a sudden increase in oxygen concentration. This is not properly captured by
333 the coarser sampling strategy (see red line in Figure 8, top). Since by that time, the oxygen
334 concentration values are in the order of the value of K_{O_2}, the non-linear limiting effect of C_{O_2}
335 in (5) plays an important role.

336 Figure 8 (bottom) shows a similar analysis of biomass growth based on the location and the
337 number of sensors used to map the oxygen concentration in the lysimeter. The variability in
338 bacterial concentration is related to the strong non-linearity in (5). As a result, there is a greater
339 sensitivity in the evaluation of bacterial growth and activity as a function of the O_2
340 concentration sampling resolution. Studies conducted at field scale are only able to record
341 spatiotemporally averaged changes, obscuring the actual dynamics. For example, Kohfahl et al.
342 (2009) modeled oxygen flux rates in groundwater during induced bank infiltration using data
343 obtained from a sampling campaign of 20 measurements in 20 months presented in Massmann
344 et al. (2008). The biogeochemical transport model of the fate of pharmaceutical components
345 during artificial recharge presented by Greskowiak et al. (2006) employed monthly data.
346 Although our study was performed in a laboratory set up and not in the field, we stress the need
347 for a fine (in space and time) sample strategy in order to link the spatial and temporal dynamics
348 of infiltration and O_2 dynamics as a function of depth.

349

6. Conclusions

This study presents the results of an experiment performed at meso-scale for monitoring infiltration rates and oxygen dynamics under an alternating sequence of wetting and drying conditions, and as a function of depth. Several conclusions may be drawn from this work:

- Infiltration rates affected by clogging revert to the initial values after a short drying period.

- Rewetting reverts drying effects and clogging recovers. Furthermore, after the first wetting period, the rate at which clogging reoccurs is faster than in the first wetting period.

- Scraping reduces clogging and the overall infiltration rate is recovered, but the effects are less pronounced than those of drying. The recovery of the infiltration rate is more effectively achieved by means of desiccation than by scraping the top soil layers.

- The alternation of short wetting and drying cycles does not have a substantial effect on microbial activity, probably because of the protective effects of the EPS surrounding the microbes.

- Oxygen stratification with depth during drying periods is due to a combination of vertical diffusion and O_2 consumption.

- The high variability of oxygen concentrations in space and time necessitates a high sampling frequency if O_2 dynamics affecting different processes are to be considered.

However, it must be ascertained whether the long drying periods offer the same benefits as short drying periods and whether our results transfer to the spatial and temporal distribution of oxygen in Managed Aquifer Recharge or induced recharge facilities.

Acknowledgements

Financial support was provided by the Ministerio de Econonía y Competitividad of the Spanish Government, projects SCARCE (CSD2009-00065) and FEAR (CGL2012-38120). This project received additional funding from the European Union's Seventh Framework Programme for research, technological development and demonstration under grant agreement no PCOFUND-GA-2008-226070. SR acknowledges the support of the Provincia Autonoma di Trento and the European Commission. We also thank Scientific and Technological centers of Universitat de Barcelona for the X-ray diffraction analysis.

References

Akhavan, M., Imhoff, P.T., Andres, A.S., Finsterle, S., 2013. Model evaluation of denitrification under rapid infiltration basin systems. J. Contam. Hydrol. 152, 18-34.

ASTM., 2000. Standard practice for classification of soils for engineering purposes (Unified Soil Classification System). ASTM standard D2487.2000 Annual Book of ASTM Standards.American Society for Testing and Materials (ASTM), Philadelphia, Pa.

Baveye, P., Vandevivere, P., Hoyle, BL., DeLeo, PC., Sanchez de Lozada, D., 1998. Environmental impact and mechanisms of the biological clogging of saturated soils and aquifer materials. Crit. Rev. Environ. Sci. Technol. 28(2), 123-191.

Bouwer, E.J., 1994. Bioremediation of chlorinated solvents using alternate electron acceptors. Handbook of Bioremediation, Boca Raton, Florida: Lewis, pp 149-175.

Bouwer, H., 1978. Groundwater Hydrology. McGraw-Hill Book Company, New York.

Bouwer, H., Rice, R.C., 1984. Renovation of wastewater at the 23rd Avenue rapid infiltration project. Water Pollut. Control Federation. 76-83.

394 Bouwer, H., Rice, R.C., 2001. Capturing flood waters for artificial recharge of groundwater. Proc
395 10th Biennial Symp Artificial Recharge of Groundwater.Hydrol. Soc. 99-106
396 Bouwer, H., 2002. Artificial recharge of groundwater: hydrogeology and engineering. Hydrogeol.
397 J. 10(1), 121-142.
398 Christensen, T.H., Bjerg, P.L.,Banwart, S.A., Jakobsen, R., Heron, G., Albrechtsen,H.J., 2000.
399 Characteristics of redox conditions in groundwater contaminant. J. Contam. Hydrol. 45(3-4),
400 165-241.
401 Constantz, J., 1982. Temperature dependence of unsaturated hydraulic conductivity of two
402 soils.Soil Sci. Soc. Am. J. 46(3), 466-470.
403 DeAngelis, K.M., Silver, W.L., Thompson, A.W., Firestone, M.K., 2010. Microbial communities
404 acclimate to recurring changes in soil redox potential status. Environ. Microbiol. 12(2),
405 3137-3149.
406 Dillon, P., 2005. Future management of aquifer recharge.Hydrogeol.J. 13(1), 313-316.
407 Dutta, T., S, Rubol., 2014. Effect of spatial heterogeneity on rate of sedimentary O_2
408 consumption reaction. In: E. Pardo-Igúzquiza et al. (eds.), Mathematics of Planet Earth,
409 Lecture Notes in Earth System Sciences, Berlin Heidelberg, pp 485-489.
410 EPA US, 1984. Process design manual for land treatment of municipal wastewater, supplement
411 on rapid infiltration and overland Flow. (EPA 625/1-81-013a).
412 Fernandez-Turiel, J.L., Gimeno, D., Rodriguez, J.J., Carnicero, M., Valero, F., 2003. Spatial and
413 seasonal variations of water quality in a Mediterranean catchment: the Llobregat River (NE
414 Spain). Environ. Geochem. Health 25(4), 453-474.
415 Fetter, C.W., 1990. Applied Hydrogeology, second ed. Columbus: Merrill Pub. Co.
416 Fox, P., Houston, A.R., Westerhoff, P., 2006. Advances in soil aquifer treatment research for
417 sustainable water reuse. AWWA Research Foundation.

418 Greskowiak, J., Prommer, H., Massmann, G., Johnston, C.D.,Nutzmann, G., Pekdeger, A., 2005.
419 The impact of variably saturated conditions on hydrogeochemical changes during artificial
420 recharge of groundwater. Appl. Geochem. 20, 1409-1426.
421 Greskowiak, J., Prommer, H., Massmann, G., Nutzmann, G., 2006. Modeling seasonal redox
422 dynamic and the corresponding fate of the pharmaceutical residue phenazone during
423 artificial recharge of groundwater. Environ. Sci. Technol. 40(21), 6615-6621.
424 Jaynes, D.B., 1990. Temperature Variations Effect on Field-Measured Infiltration. Soil Science
425 Soc. Am. J. 54(2), 305-311.
426 Kohfahl, C., Massmann, G., Pekdeger, A., 2009. Sources of oxygen flux in groundwater during
427 induced bank filtration at a site in Berlin, Germany. Hydrogeol. J. 17(3), 571-578.
428 Krause, S., Boano, F., Cuthbert, M.O., Fleckenstein, J.H., Lewandowski, J., 2014. Understanding
429 process dynamics at aquifer-surface water interfaces: An introduction to the special section
430 on new modeling approaches and novel experimental technologies. Water Resour. Res.
431 50(2), 1847-1855.
432 Le Bihan, Y., Lessard, P., 2000. Monitoring biofilter clogging: biogeochemical characteristics of
433 the biomass. Water Res. 34(17), 4284-4294.
434 Massmann, G., Nogeitzig, A., Taute, T., Pekdeger, A., 2008. Seasonal and spatial distribution of
435 redox zones during lake bank filtration in Berlin, Germany. Environ. Geology 54(1), 53-65.
436 McCarty, L., Semprini, P.L., 1994. Ground-water treatment for chlorinated solvents. Handbook
437 of Bioremediation, Boca Raton, Florida: Lewis, pp 87-116.
438 McClain, M.E., Boyer, E.W., Dent, C.L., Gergel, S.E., Grimm, N.B., Groffman, P.M., Hart, S.C.,
439 Harvey, J.W., Johnston, C.A., Mayorga, E., McDowell, W.H., Pinay, G., 2003. Biogeochemical
440 hot spots and hot moments at the interface of terrestrial and aquatic ecosystems.Ecosyst.
441 6(4), 301-312.

442 Millington, R.J., Quirk, J., 1961. Permeability of porous solids.Trans. Faraday Soc.
443 57, 1200-1207.
444 Mousavi, S.F., Rezai, V., 1999. Evaluation of scraping treatments to restore initial infiltration
445 capacity of three artificial recharge projects in central Iran. Hydrogeol. J. 7(5), 490-500.
446 Neale, C., Hughes, J.B., Ward, C.H., 2000. Impacts of unsaturated zone properties on oxygen
447 transport and aquifer rearetaion. Ground Water 38(5), 784-794.
448 NRMRI, 2006.Process design manual; Land treatment of municipal wastewater effluents.
449 Or, D., Phutane, S., Deschene, A., 2007. Extracellular polymeric substances affecting pore-scale
450 hydrologic conditions for bacterial activity in unsaturated soils.Vadose Zone J. 6, 298–305.
451 Pedretti, D., Barahona-Palomo, M., Bolster, D., Fernàndez-Garcia, D., Sanchez-Vila, X.,
452 Tartakovsky, D.M., 2012. Probabilistic analysis of maintenance and operation of artificial
453 recharge ponds. Advances Water Resour. 36, 23–35.
454 Rifai, H.S., Borden, R.C., Wilson, J.T., Ward, C.H., 1995. Intrinsic bioattenuation for subsurface
455 restoration. Intrinsic bioremediation 1-29.
456 Roberson, E.B., Firestone, M.K., 1992. Relationship between dessication and exopolysaccharide
457 production in a soil Pseudomonas sp. Appl. Environ.Microbiol.58(4), 1284–1291.
458 Romaní, A.M., Guasch, H., Muñoz, I., Ruana, J., Vilalta, E., Schwartz, T., Emtiazi, F., Sabater, S.,
459 2004. Biofilm structure and function and possible implications for riverine DOC
460 dynamics.Microb. Ecol. 47(4), 316-328.
461 Rubol, S., Silver, W.L., Bellin, A., 2012. Hydrologic control on redox and nitrogen dynamics in a
462 peatland soil. Sci. Total Environ. 432, 37-46.
463 Rubol, S., Manzoni, S., Bellin, A., & Porporato, A., 2013. Modeling soil moisture and oxygen
464 effects on soil biogeochemical cycles including dissimilatory nitrate reduction to ammonium
465 (DNRA). *Advances in Water Resources*, *62*, 106-124.

Rubol,S., Freixa, A., Carles-Brangarí, A., Fernàndez-Garcia, D., Romaní, A.M., Sanchez-Vila, X., 2014. Connecting bacterial colonization to physical and biochemical changes in a sand box infiltration experiment. Hydrogeolog. J. 517, 217-327.

Schimel, J., Balser, T.C., Wallenstein, M., 2007. Microbial stress-response physiology and its implications for ecosystem function.Ecol. 88(6), 1386-1394.

Schmidt, C.M., Fisher, A.T., Racz, A.J., Lockwood, B.S., Huertos, M.L., 2011. Linking denitrification and infiltration rates during managed artificial recharge. Environ. Sci. Technol. 45(22), 9634-9640.

Shaler, T.A., Klecka, G.M., 1986. Effects of dissolved oxygen concentration on biodegradation of 2,4-dichlorophenoxyacetic acid. Appl. Environ. Microbiol. 51, 950–955.

Thullner, M., Zeyer, J., Kinzelbach, W. 2002. Influence of microbial growth on hydraulic properties of pore networks. Transport in Porous Media 49, no. 1: 99–122.

Vandevivere, P., and Baveye, P., 1992. Effect of bacterial extracellular polymers on the saturated hydraulic conductivity of sand columns. Appl. Environ. Microbiol. 58(5), 1690-1698.

Vogel, T., 1994. Natural bioremediation of chlorinated solvents. Handbook of Bioremediation, Boca Raton, Florida: Lewis, pp 201-225.

Zhang, Q., Yan, T., 2012. Correlation of intracellular Trehalose concentration with desiccation resistance of soil Escherichia coli populations, Appl. Environ.Microbiol. 78 (20), 7407–7413.

Table 1. Composition of the synthetic water used in the infiltration experiment (in mg/L).

Na^+	K^+	Ca^{2+}	Mg^{2+}	Cl^-	$NO3^-$	$SO4^{2-}$	$HCO3^-$	$NH4^+$	$PO4^{3-}$	$SiO3^{2-}$	Cellobiose	Leucine-proline	Humic acid
159.3	39.9	120.2	34.0	343.9	12.1	202.7	145.2	1.7	1.0	12.5	1.5	1.5	7.0

Table 2. Information about the duration of the individual cycles in the experiment

Cycle	Abbreviation	Length
First wetting cycle	W1	5d 11h
First drying cycle	D1	7d 13h
Second wetting cycle	W2	6d 6h
Second drying cycle	D2	7d 18h
Third wetting cycle	W3a	7d 12h
	W3b	6d 14h
Third drying cycle	D3	25d 22h
Fourth wetting cycle	W4	2d 8h
Fourth drying cycle	D4	4d 17h
Fifth wetting cycle	W5	10d 23h

Fifth drying cycle	D5	1h

499

500

501

502

503 **Table 3.** Characteristics of the sediments

pH	OC(%)	NH4-N (mg-N/Kg)	NO3-N (mg-N/Kg)	Medium sand(%)	Fine sand(%)	Finer material (%)
7.6	2	2	5	81.8	17.67	0.52

504

505

506

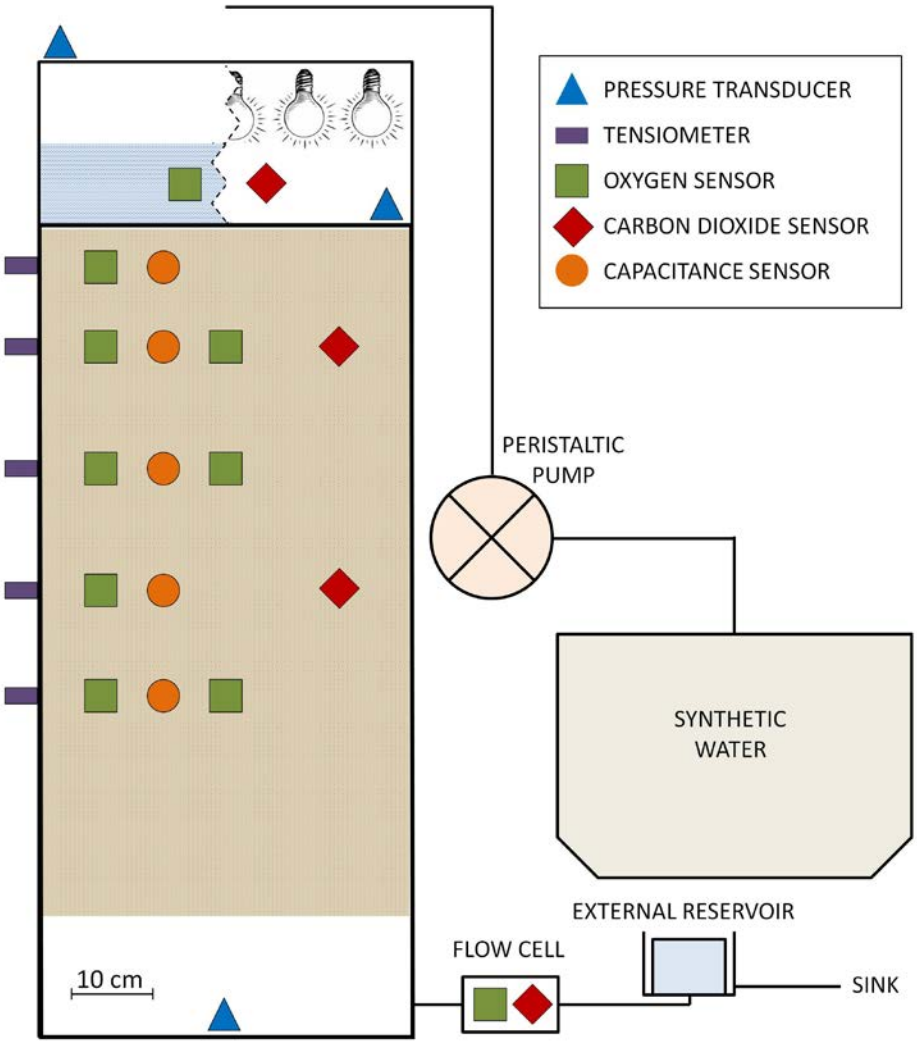

507

508 **Figure 1.**Sketch of the experimental setup showing the body of the lysimeter, the location of the
509 sensors and input/output water systems. The boundary condition active during wetting is a
510 constant ponding (left side of the tank) and light bulbs during drying periods (right side in the
511 ponding area).

512

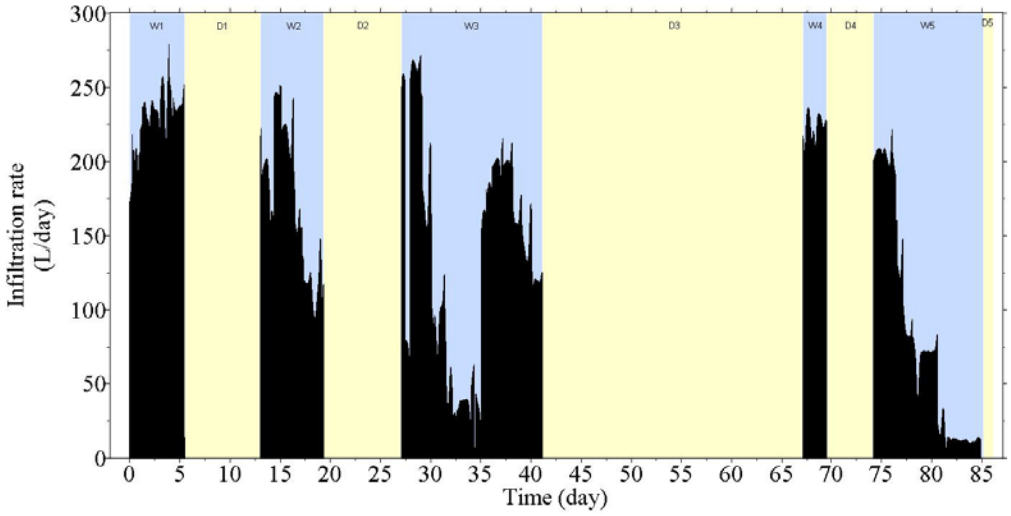

513

514 **Figure 2.** Evolution of the infiltration rate (in L/day) with time during the experiment. Blank

515 areas correspond to drying phases.

516

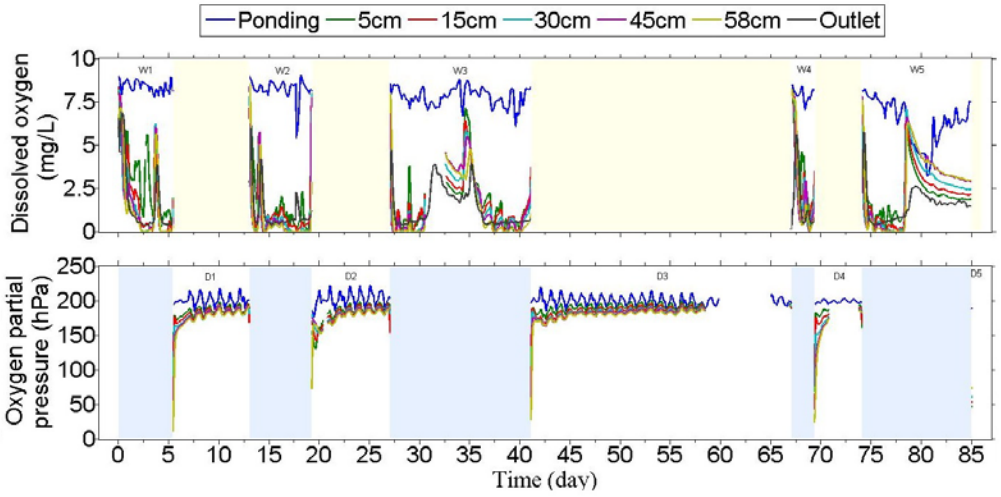

517

518 **Figure 3.** O_2 concentration at the ponding and at different depths of soil across the vertical

519 length of the lysimeter during wetting (measured as dissolved oxygen in mg/L) and drying cycles

520 (measured as oxygen partial pressure in hPa). The values at depths 15, 30 and 58 correspond to

the arithmetic average of the duplicate sensors. The reported sampling variances are ($\sigma^2_{15cm} = 0.015$, $\sigma^2_{30cm} = 0.008$, $\sigma^2_{58cm} = 0.013$).

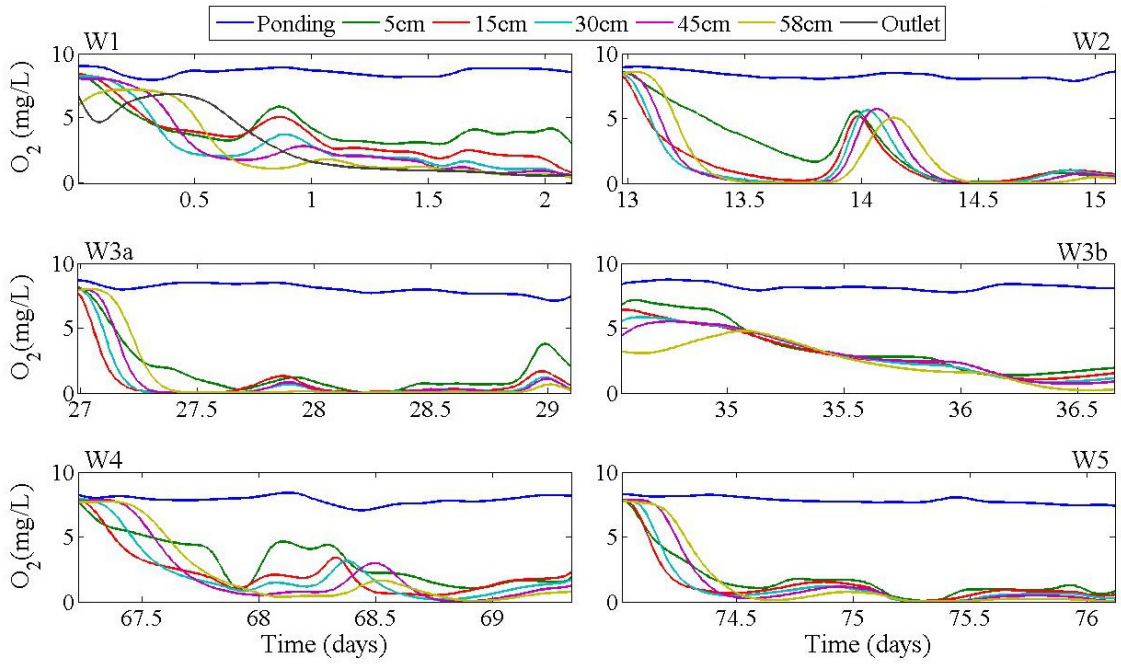

Figure 4. O_2 concentration dynamics at the start of each wetting cycle; plots report the changes during the first two days of each wetting cycle (from W1 to W5). The values at depths 15, 30 and 58 correspond to the arithmetic average of the duplicate sensors. The sampling variances are ($\sigma^2_{15cm} = 0.015$, $\sigma^2_{30cm} = 0.008$, $\sigma^2_{58cm} = 0.013$).

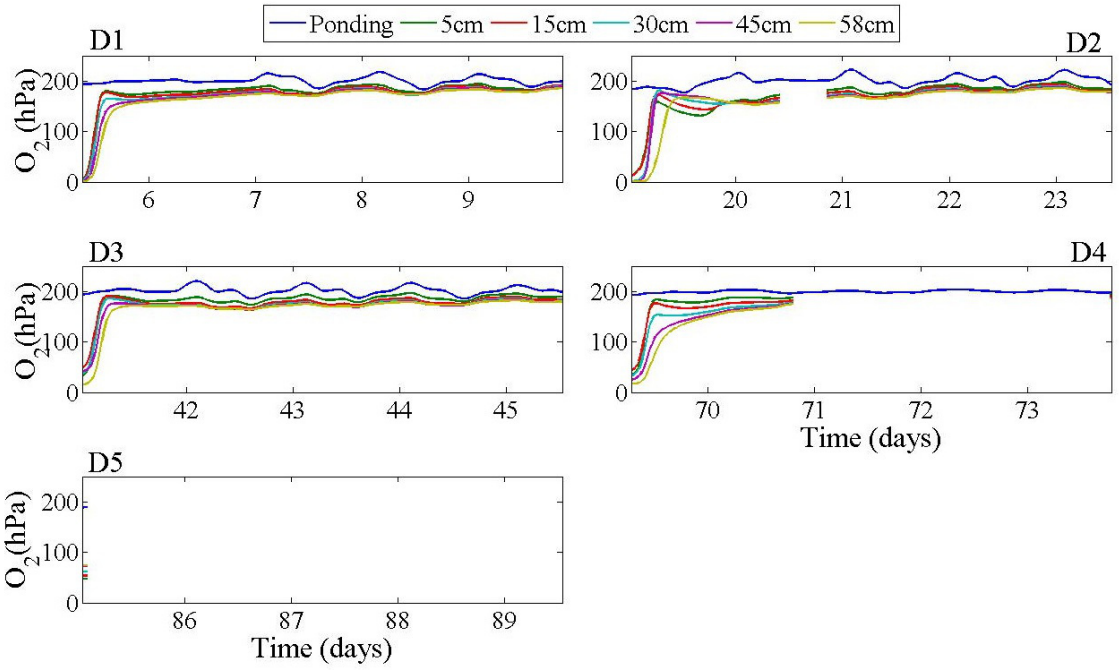

531

532 **Figure 5.** Dynamics of O_2 at the start of each drying cycle for 5 days (D5 lasted only 1h). The

533 values at depths 15, 30 and 58 correspond to the arithmetic average of the duplicate sensors.

534 The sampling variances are ($\sigma^2_{15cm} = 0.015$, $\sigma^2_{30cm} = 0.008$, $\sigma^2_{58cm} = 0.013$).

535

536

537

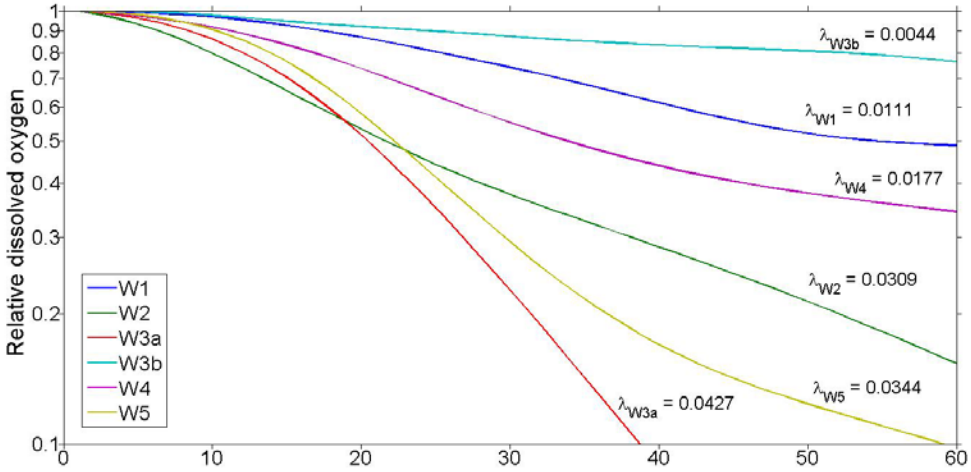

538

539 **Figure 6.** Relative dissolved oxygen concentration at the start of each wetting cycle. Oxygen

540 depletion is a function of both transport and consumption mechanisms. Parameter λ is the

541 decay parameter in a negative exponential function.

542

543

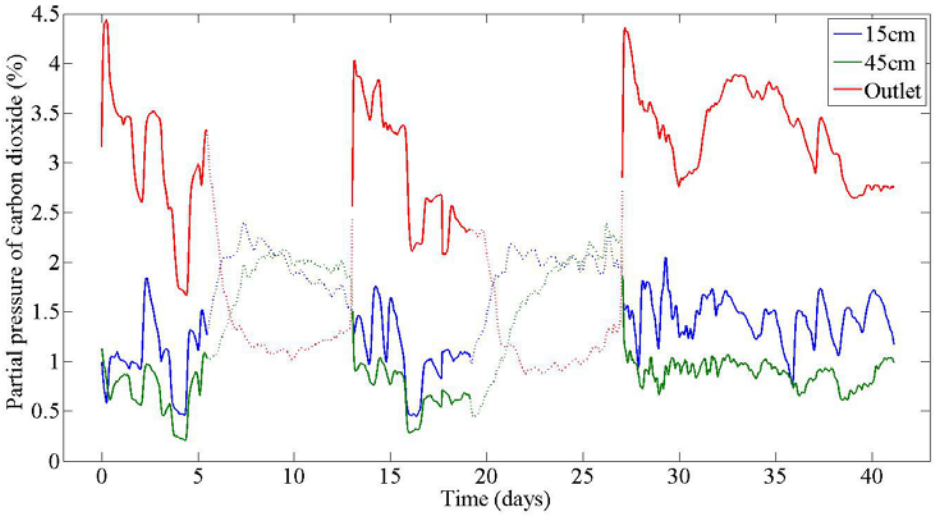

544

545 **Figure 7.** Partial pressure of CO_2 (%pCO_2) during wetting (solid lines) and drying cycles (dotted

546 lines). CO_2 sensor requires 99% humidity for proper functioning, so data during drying cycles are

547 not shown.

548

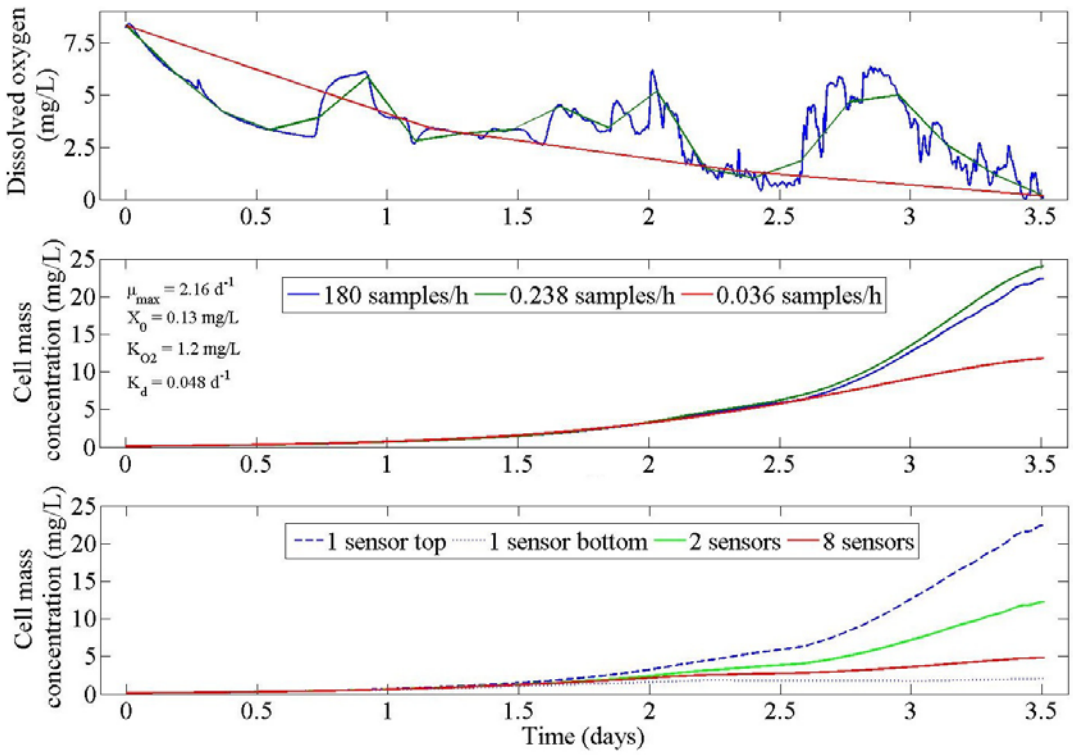

549

550 **Figure 8.** Top: Dissolved oxygen concentration dynamics during the first 3.5 days of W1.

551 Different lines depict measurements from specific monitoring resolution strategies: 180

552 samples/hour in blue, 0.238 samples/hour in green, and 0.036 samples/hour in red. Middle: Cell

553 biomass concentrations estimated from (5) considering oxygen as the growth-limiting factor

554 corresponding to the three sampling densities. Bottom: Biomass concentration growth deduced

555 from (5) by using the data obtained in individual sensors or in a combination of them.

556